Studies of Real and Virtual Photon Structure at HERA.

T. McMahon
Oliver Lodge Laboratory,
University of Liverpool, Liverpool, England

For the H1 and ZEUS Collaborations

Recent results of real and virtual photon structure from the H1 and ZEUS collaborations are discussed. Jet cross-sections in photoproduction processes provide new constraints on the real photon parton densities. Measurements of dijet cross-sections in deep-inelastic scattering show clear evidence for a resolved component to the virtual photon which is suppressed with increasing photon virtuality. The first measurement of the effective parton density of the virtual photon is presented. A study of the properties of the virtual photon remnant is also shown.

1 Introduction

The cross-section for high transverse momentum (P_t) jet production in ep collisions is dominated by processes in which the exchanged photon is quasi-real (photoproduction processes). In leading order, two types of interaction can be distinguished: direct processes, where the photon couples as a point-like object to a parton from the proton, and resolved processes, where a parton from the photon carrying a fraction x_γ of its momentum interacts with a parton from the proton. Resolved events will contain a photon remnant in addition to the proton remnant, and there is the possibility of remnant-remnant interactions. The photoproduction jet cross-section is sensitive to the density of partons in the photon at the scale P_t^2 of the jets.

In deep-inelastic scattering (DIS) processes, where the virtuality of the exchanged photon (Q^2) is non-zero, the production of high P_t jets is usually dominated by direct processes. However, if the virtual photon is probed with sufficiently high resolution ($P_t^2 >> Q^2$) the cross-section will still be sensitive to the photon parton density. As Q^2 increases at fixed P_t^2 perturbative QCD predicts that the parton density of the photon should be suppressed and that the structure should simplify to the direct coupling to a $q\bar{q}$ pair.

The data presented here was taken during 1995 and 1996 when HERA was colliding 27.5 GeV positrons with 820 GeV protons.

2 Photoproduction Jet Cross-section

The ZEUS collaboration has performed a measurement of the di-jet cross-section in photoproduction as a function of E_T, the transverse energy of the highest E_T jet and the pseudorapidities [a], η, of the two jets [1]. Jets were defined using the longitudinally invariant k_t algorithm [2]. Events

[a] Defined by $\eta = -\ln \tan \frac{\theta}{2}$ with the polar angle θ defined with respect to the incident proton direction.

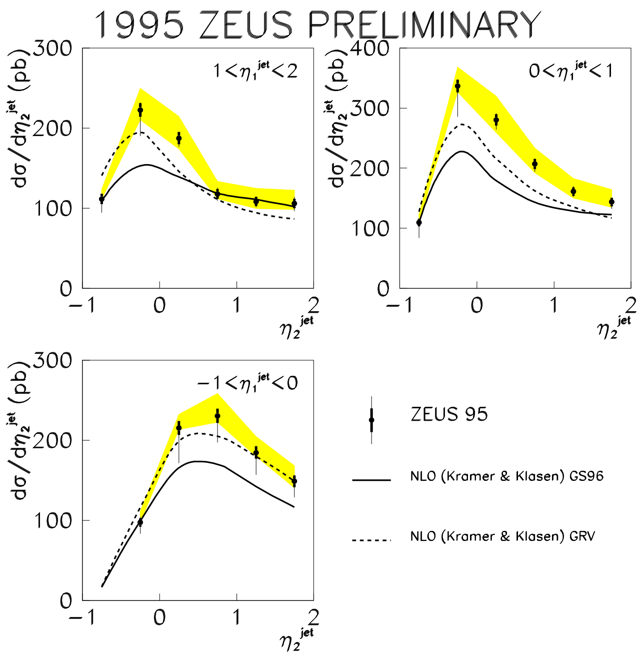

Figure 1: The dijet cross-section $d\sigma/d\eta_2^{\rm jet}$ in different regions of $\eta^{\rm jet1}$ for photoproduction events. The thick error bars show the statistical error and the total error bar represents the quadratic sum of statistical and systematic uncertainties. The shaded band represents the error due to the uncertainty in the calorimeter energy scale.

were selected with $E_T > 14\,{\rm GeV}$, $E_T^{\rm jet2} > 11\,{\rm GeV}$ and $-1 < \eta_{1,2}^{\rm jet} < 2$. Figure 1 shows the cross-section $d\sigma/d\eta_2^{\rm jet}$ for $212 < W < 277\,{\rm GeV}$, where W is the γP centre-of-mass energy. In this kinematic region, the data are sensitive to the photon parton densities at low x_γ and the proton parton densities are well constrained. The data are divided into three regions of η_1^{jet}: $-1.0 < \eta_1^{\rm jet} < 0.0$, $0.0 < \eta_1^{\rm jet} < 1.0$ and $1.0 < \eta_1^{\rm jet} < 2.0$. and are compared to NLO calculations from Klasen and Kramer using the GS96 and the GRV-HO parameterisations of the photon parton densities. The measured cross-sections in the central pseudorapidity region are higher than both predictions but for each $\eta_1^{\rm jet}$ region the measurements are close to the NLO calculations in the smallest $\eta_2^{\rm jet}$ bin.

Hadronisation corrections have been estimated to be largest in the most negative η_2^{jet} bin of each η_1^{jet} range and elsewhere are smaller than the experimental error. The uncertainty due to the factorisation and renormalisation scale used in the NLO calculations has been estimated to be of order 10%.

These data are able to provide new constraints on the parton density of the real photon.

3 Virtual Photon Structure

3.1 Deep-Inelastic Scattering Jet-Cross-Section

A measurement has been made by the H1 collaboration of the triple-differential dijet cross-section [3] $d^3\sigma/dQ^2 d\bar{E}_t^{\,2} dx_\gamma^{jets}$, where Q^2 is the virtuality of the photon, $\bar{E}_t^{\,2}$ is the mean of the transverse energies of the two highest E_t jets measured in the $\gamma^* P$ mass frame and x_γ^{jets} is the value of x_γ reconstructed from the jets:

$$x_\gamma^{jets} = \frac{\sum_{jets}(E^{jet} - p_z^{jet})}{\sum_h (E^h - p_z^h)} \qquad (1)$$

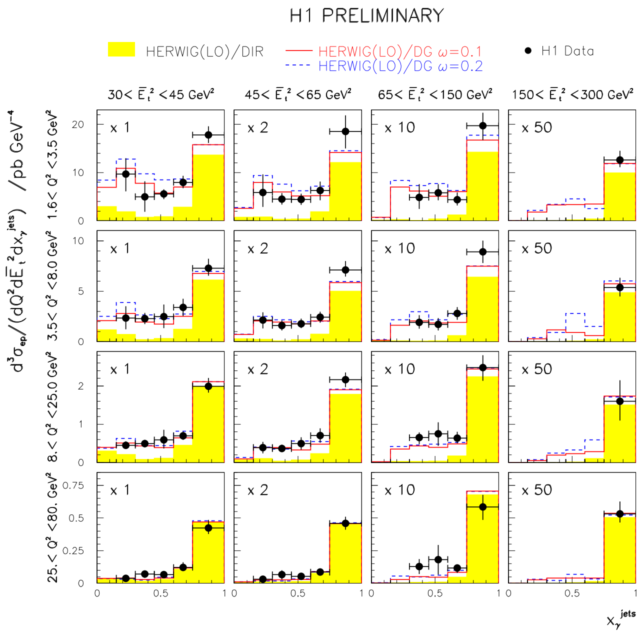

Figure 2: The differential dijet cross-section $d^3\sigma/dQ^2 d\bar{E}_t{}^2 dx_\gamma^{jets}$ as a function of x_γ^{jets} in different regions of $\bar{E}_t{}^2$ and Q^2. The scale factors applied to the cross-sections are indicated. Also shown are the predictions from a LO model including a resolved component to the virtual photon (dotted and dashed histograms) and the direct photon component of this model (shaded histogram).

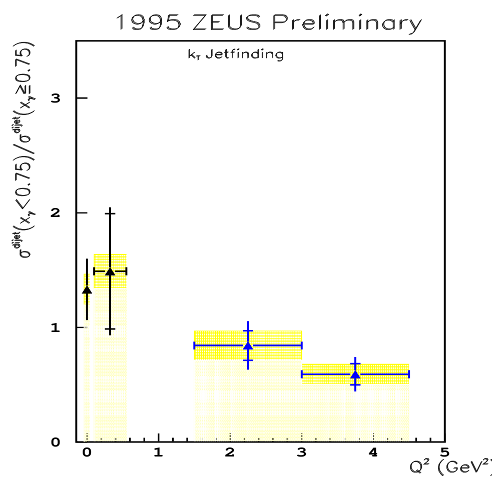

Figure 3: The ratio $\frac{\sigma(x_\gamma^{jets}<0.75)}{\sigma(x_\gamma^{jets}>0.75)}$ as a function of Q^2. The inner error bars indicate the statistical contribution to the error. The band represents the systematic error due to the uncertainty in the energy scale of the calorimeter.

where the sum in the denominator is over all final state particles except the scattered positron. The data cover the kinematic range $1.6 < Q^2 < 80\text{GeV}^2$ in virtuality and $0.1 < y < 0.7$ in inelasticity. Jets were reconstructed using the longitudinally invariant k_T algorithm [2]. Events were selected if the two highest E_t jets satisfied the following cuts: $|\ \eta_1^{jet} - \eta_2^{\text{jet}}\ | < 1.0, -3.0 < \bar{\eta} < -0.5$, $\bar{E}_t{}^2 > 30\,\text{GeV}^2$ and $\frac{|(E_t^{\text{jet1}} - E_t^{\text{jet2}})|}{(E_t^{\text{jet1}} + E_t^{\text{jet2}})} < 0.25$.

Figure 2 shows the di-jet cross-section as a function of x_γ^{jets} for different ranges of $\bar{E}_t{}^2$ and Q^2. The absence of a data point indicates that no measurement was made in that bin due to insufficient statistics. The x_γ^{jets} distribution peaks towards $x_\gamma^{jets} = 1$ where the direct photon contribution is concentrated. The data are compared with the predictions from a LO model [4] which contains only the direct photon contribution (shaded histogram) and from the same model after including a resolved contribution for the photon which is suppressed with increasing Q^2 in a manner motivated by perturbative QCD [5]. The data show the need for a significant resolved contribution everywhere except where $Q^2 > \bar{E}_t{}^2$ and it is no longer expected that structure in the virtual photon can be resolved. By including a resolved component to the virtual photon which is suppressed with increasing Q^2 a reasonable description of the data is achieved.

A measurement [6] has been performed by the ZEUS collaboration of the ratio of the resolved to the direct jet cross-section defined as:

$$R = \frac{\sigma(x_\gamma^{jets} < 0.75)}{\sigma(x_\gamma^{jets} > 0.75)} \tag{2}$$

for $0.2 < y < 0.55$ and x_γ^{jets} defined according to equation 1. Jets were found using the k_t algorithm [2] and events were required to have at least two jets with $E_T^{jet} > 6.5$ GeV and

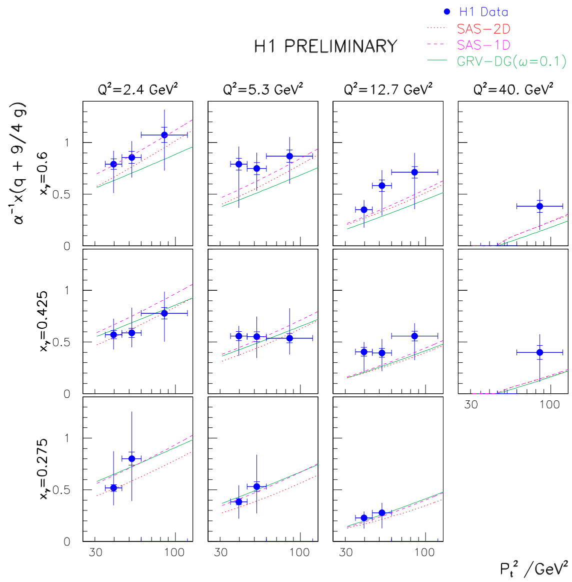

Figure 4: The leading order effective parton density of the photon $x_\gamma \tilde{f}_\gamma$, divided by the fine structure constant α, as a function of P_t^2 for different values of Q^2 and x_γ.

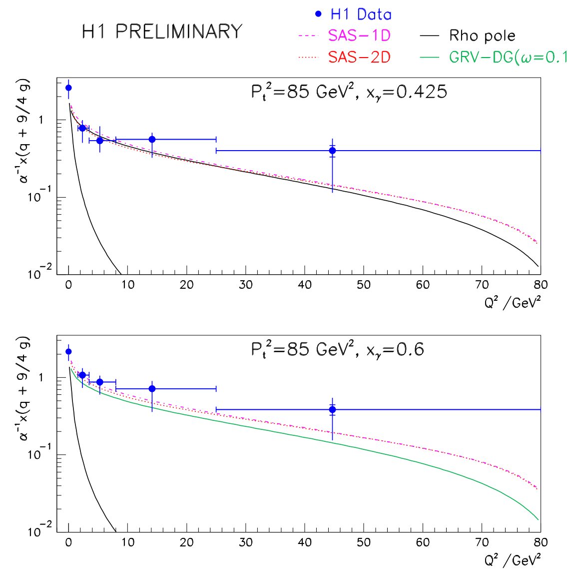

Figure 5: The leading order effective parton density of the photon $x_\gamma \tilde{f}_\gamma$, divided by the fine structure constant α, as a function of Q^2 for different values of x_γ and $P_t^2 = 85\,\mathrm{GeV}^2$.

$-1.125 < \eta^{jet} < 1.875$. Figure 3 shows that R decreases with increasing Q^2 consistent with the suppression of the photon parton density.

3.2 Effective Parton Density of Virtual Photon

The Single Effective Subprocess Approximation[7] has been utilised to extract the effective parton density of the virtual photon from the H1 dijet cross-sections[3]. The effective parton density is defined as:

$$\tilde{f}_\gamma(x_\gamma, P_t^2, Q^2) = \sum_{n_f} (f_{q/\gamma}(x_\gamma, P_t^2, Q^2) + f_{\bar{q}/\gamma}(x_\gamma, P_t^2, Q^2)) + \frac{9}{4} f_{g/\gamma}(x_\gamma, P_t^2, Q^2) \tag{3}$$

where the $f_{i/\gamma}$ are averaged over the polarisation states of the virtual photon.

The measured effective parton density as a function of the probing scale P_t^2 for different values of x_γ and Q^2 is shown in figure 4. Only points where $\langle P_t^2 \rangle > \langle Q^2 \rangle$ are shown. The scale dependence contrasts with the falling behaviour expected for hadronic parton densities and, within the large systematic errors, is consistent with the logarithmic scale dependence predicted by perturbative QCD for the point-line coupling of the photon to a $q\bar{q}$ pair. The data are compared with several QCD inspired parameterisations[5,8] which are all in reasonable agreement with the measured values.

Figure 5 shows the Q^2 evolution of the effective parton density for $P_t^2 = 85\,\mathrm{GeV}^2$ and two ranges of x_γ. A clear Q^2 suppression can be seen. Again the QCD inspired parameterisations which predict a logarithmic suppression with Q^2 are in reasonable agreement with the data. Also shown is the form of the suppression characteristic of the Vector Dominance Model[b] which is clearly ruled out by the data.

[b] $f_{i/\gamma}(Q^2, P_t^2, x_\gamma) \sim f_{i/\gamma}(0, P_t^2, x_\gamma)(\frac{m_\rho^2}{m_\rho^2+Q^2})^2$

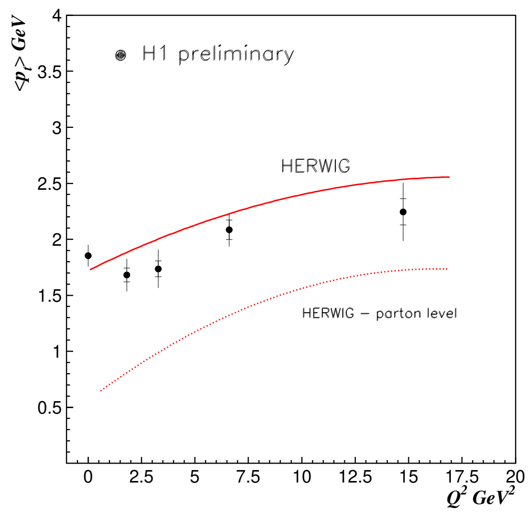

Figure 6: The Q^2 dependence of the $\langle P_t \rangle$ of the photon remnant. The data (points) are compared to a LO simulation before (dotted line) and after (solid line) hadronisation.

3.3 Properties of Virtual Photon Remnant

An analysis of the photon remnant jet has been performed by H1 for photoproduction data and DIS data with $1.4 < Q^2 < 25\,\text{GeV}^2$. Each event is decomposed into 4 jets (two high E_t jets and two remnants) using the DECO [9] jet algorithm. The jet with the most negative p_z in the $\gamma^* P$ cms frame is defined as the candidate photon remnant jet. The two high E_t jets must satisfy the cuts: $p_T > 5\,\text{GeV}$, $-3 < \eta < 0$, $p_T^{(1)} + p_T^{(2)} > 12\,\text{GeV}$ and $\mid (\phi_1 - \phi_2) \mid > 2$ rad. To enrich the sample with resolved events, it is required that $x_\gamma^{jets} < 0.75$.

Figure 6 shows the corrected $\langle P_t \rangle$ of the photon remnant jet as a function of Q^2. The data show a weak increase with increasing Q^2. Also shown are the predictions from a LO simulation [4] which assumes that the intrinsic k_t in the remnant is a gaussian distribution $dN/dp_T^2 \sim e^{(-k_T^2/k_0^2)}$ with $k_0 = 0.66$ GeV which is able to describe the observed dependence on a qualitative level. The shape of the Q^2 dependence was found to be unaffected by hadronisation effects.

References

1. ZEUS Collaboration, Contributed Paper to XXIX International Conference on High Energy Physics, Vancouver, July 1998
2. S.D. Ellis and D.E. Soper, *Phys. Rev.* D **48**, 3160 (1993)
   S. Catani *et al*, *Nucl. Phys.* B **406**, 187 (1993)
3. H1 Collaboration, *'Measurement of Dijet Cross-Sections at Low Q^2 and the Extraction of an Effective Parton Density of the Virtual Photon'*, DESY-98-205, to be published in Eur. Phys. J.C
4. G. Marchesini *et al*, Comp. Phys. Comm. **67**, 465 (1992)
5. M.Drees and R. Godbole, *Phys. Rev.* D **50**, 3124 (1994)
6. ZEUS Collaboration, Contributed Paper to XXIX International Conference on High Energy Physics, Vancouver, July 1998
7. B.V. Combridge and C.J. Maxwell, *Nucl. Phys.* B **239**, 429 (1984)
8. T. Sjöstrand and G.A. Schuler *Phys. Lett.* B **376**, 193 (1996)
9. A. Valkarova and G. Knies, DESY-94-047(1994)